CHALMERS
UNIVERSITY OF TECHNOLOGY

Advancing Electrophoretic Deposition for Multifunctional Structural Batteries

Master's thesis in Materials Engineering

GUOKANG LI

DEPARTMENT OF INDUSTRIAL AND MATERIALS SCIENCE
CHALMERS UNIVERSITY OF TECHNOLOGY
Gothenburg, Sweden 2025
www.chalmers.se

Master's thesis 2025

Advancing Electrophoretic Deposition for Multifunctional Structural Batteries

GUOKANG LI

CHALMERS
UNIVERSITY OF TECHNOLOGY

Department of Industrial and Materials Science
Division of Material and Computational Mechanics
Chalmers University of Technology
Gothenburg, Sweden 2025

Advancing Electrophoretic Deposition for Multifunctional Structural Batteries
GUOKANG LI

Supervisor: Leif Asp & Richa Chaudhary & Varun Chaudhary, Department of In dustrial and Materials Science
Examiner: Leif Asp, Department of Industrial and Materials Science

Master's Thesis 2025
Department of Industrial and Materials Science
Division of Material and Computational Mechanics
Chalmers University of Technology
SE-412 96 Gothenburg
Telephone +46 76 154 9236

Cover: Conceptual illustration of a futuristic electric vehicle incorporating carbon fibre-based structural battery components in the roof and front body panels. These multifunctional elements enable both load-bearing capability and energy storage.

Typeset in LaTeX
Printed by Chalmers Reproservice
Gothenburg, Sweden 2025

Advancing Electrophoretic Deposition for Multifunctional Structural Batteries
GUOKANG LI
Department of Industrial and Materials Science
Chalmers University of Technology

Abstract

This thesis presents a comprehensive study on the application of electrophoretic deposition (EPD) for the fabrication of multifunctional cathode electrodes in structural batteries. Structural batteries are emerging as a promising class of energy systems capable of combining mechanical and electrochemical functions in a single architecture. Such dual-purpose capability is of growing interest in sectors where lightweight design and space efficiency are critical, such as aerospace, automotive, and portable electronics. In this context, EPD was selected as the core fabrication method due to its advantages in process scalability, material versatility, and the ability to directly deposit active materials onto conductive structural substrates such as carbon fibres (CF).

The study was divided into four major experimental paths: (1) enhancement of deposition quality through magnetic field assistance during the EPD process; (2) improvement of manufacturing efficiency via a redesigned high-throughput electrode holder; (3) extension of EPD application to electromagnetic interference (EMI) shielding by depositing Fe_3O_4-based composites; and (4) evaluation of electrochemical performance through controlled variation of reduced graphene oxide (rGO) content in LFP-based cathode formulations. While magnetic fields were not the main focus of this work, their selective application during deposition and drying stages proved effective in improving coating uniformity and reducing agglomeration under certain composition conditions.

To explore multifunctionality beyond energy storage, Fe_3O_4 was introduced as a magnetic filler material in the EPD suspension to fabricate EMI shielding electrodes. Although EMI shielding effectiveness was not evaluated due to time limitations, the successful deposition of Fe_3O_4-based coatings on CF substrates supports the feasibility of EPD for future dual-functional applications. In parallel, the study evaluated electrochemical performance using half-cell pouch assemblies, tested through open circuit voltage (OCV), cyclic voltammetry (CV), electrochemical impedance spectroscopy (EIS), and galvanostatic cycling. The results indicated that moderate additions of rGO improve internal resistance and electrode kinetics, while excessive carbon additives adversely affect coating consistency and dispersion.

Overall, this work demonstrates the adaptability and versatility of EPD in fabricating structural battery electrodes, while proposing pathways for integrating electromagnetic and electrochemical functionality. The results provide practical insights for future research and development of multifunctional power systems, laying a solid foundation for scalable, lightweight energy solutions in advanced engineering applications.

Keywords: EPD, Carbon fibre composites, Lithium-ion batteries, Structural batteries, High-throughput, EMI shielding.

Acknowledgements

I would like to express my sincere gratitude to everyone who has supported and guided me throughout the course of this thesis project. This work would not have been possible without the encouragement, insights, and contributions of many individuals.
First and foremost, I am deeply thankful to my examiner, Professor Leif Asp, for his inspiring perspective and kind mentorship. Despite a demanding schedule, he always took time to provide thoughtful feedback and generous guidance. His warm presence and intellectual enthusiasm made every meeting both productive and motivating, and I am truly grateful for his support throughout this journey.
My heartfelt thanks also go to my supervisor, Dr. Richa Chaudhary, whose dedication, patience, and encouragement have been fundamental to the development of this work. From the very beginning, her clear guidance and willingness to discuss every challenge with care and precision helped me stay focused and motivated. I am also particularly grateful for the professional insights and advice she shared, which will undoubtedly shape my future path in research.
I would also like to extend my sincere appreciation to my co-supervisor, Professor Varun Chaudhary, for his continuous support and valuable input throughout the project. His technical expertise and thoughtful feedback helped me refine my work and think more critically, especially during key phases of the research.
In addition, I would like to thank the entire Division of Material and Computational Mechanics at Chalmers University of Technology for providing a supportive and stimulating environment in which to carry out my thesis. Special thanks to Huixin Chen for the engaging discussions, kind assistance, and the sense of community she helped create, both in and outside the lab.

I am also very grateful to my close friends Jihui Yang and Nicklas Ishøy for accompanying me throughout these two years of the master's journey. I sincerely wish both of them all the best in their future endeavours.
Special thanks go to my friend Xiaojun Zhu, a master's student at the Department of Architecture at Chalmers, who generously provided professional assistance in the 3D printing of experimental tools during a critical stage of my research. Her expertise significantly accelerated the experimental progress.
I would like to express my deepest gratitude to my best soul mate Xuerui Mi, who stood by me through the most difficult moments of my studies. Her unwavering encouragement and support were instrumental in helping me complete this academic journey. I wish her every success and happiness, and may we always remain true soul companions.
Lastly, I want to thank my beloved family for their endless support and understanding throughout my academic and personal life. Their care and belief in me have been a constant source of strength. I wish them health, peace, and happiness in everything ahead.

"Every end is a new beginning."

Guokang Li, Gothenburg, June 2025

List of Acronyms

Below is the list of acronyms that have been used throughout this thesis listed in alphabetical order:

EPD	Electrophoretic Deposition
CF	Carbon Fibres
LFP	Lithium Iron Phosphate
CB	Carbon Black
rGO	Reduced Graphene Oxide
PDDA	Poly(diallyldimethylammonium chloride)
EtOH	Ethanol
DC	Direct Current
EMI	Electromagnetic Interference
CV	Cyclic Voltammetry
EIS	Electrochemical Impedance Spectroscopy
GCD	Galvanostatic Charge–Discharge
OCV	Open Circuit Voltage
SB	Structural Battery
SBC	Structural Battery Composite
SBE	Structural Battery Electrolyte
SEM	Scanning Electron Microscopy
ESEM	Environmental Scanning Electron Microscopy
XRD	X-Ray Diffraction
NMC	Lithium Nickel Manganese Cobalt Oxide
LIB	Lithium-Ion Battery
VNA	Vector Network Analyzer
HTM	High-throughput method

Nomenclature

Below is the nomenclature of indices, sets, parameters, and variables that have been used throughout this thesis.

Indices

n	Number of electrons transferred
t	Time index

Sets

`F1-F5`	Set of electrode formulations
`KK58-KK93`	Set of electrode sample IDs

Parameters

A	Electrode area (cm^2)
C	Bulk concentration (mol/cm^3)
F	Faraday's constant (96,485 C/mol)
I	Applied current (A)
m	Active material mass (g)
Q	Charge capacity (C)
Q_{nominal}	Nominal capacity
Q_{sp}	Specific capacity

Variables

E	Electrode potential (V)
E^0	Standard electrode potential (V)

$E^{0'}$	Formal potential (V)
E_{pa}	Anodic peak potential (V)
E_{pc}	Cathodic peak potential (V)
ΔE_p	Peak separation (V)
i_{pa}	Anodic peak current (A)
i_{pc}	Cathodic peak current (A)
i_p	Peak current (A)

Contents

List of Figures

List of Tables

1

Introduction

"The best way to predict the future is to invent it."

— Alan Kay

Throughout human history, innovation and development have always been the driving forces behind societal progress. From the early Agricultural Revolution to the later Industrial Revolution, humanity has continuously broken through technological barriers, transforming the way we live. The Industrial Revolution marked a turning point—the steam engine replaced human labour with machines, and factories transformed production. Later, the internal combustion engine revolutionised transportation with cars and aeroplanes. In the 20th century, computers and the internet sparked the Information Age, while recent advances in artificial intelligence have opened new possibilities for the future. At the same time, humanity's use and storage of energy have also been evolving. Early energy storage methods were simple, such as using water wheels or windmills to store mechanical energy. In the 19th century, the invention of lead-acid batteries opened a new era of electrochemical energy storage [1]. By the late 20th century, the emergence of lithium-ion batteries revolutionised energy storage, making portable devices like mobile phones and laptops possible, while also laying the foundation for the large-scale application of electric vehicles and renewable energy. Lithium-ion batteries have undergone rapid development and are now widely used across various applications; nevertheless, state-of-the-art lithium-ion batteries still face significant limitations [2] [3]. Issues such as excessive weight, limited energy density, and safety concerns continue to restrict the range and efficiency of transportation, thereby hindering further progress in the field. Significant efforts and numerous experiments have been dedicated to developing batteries that offer both enhanced safety and higher energy density. These challenges, however, may be effectively addressed by the innovative concept of structural batteries, which integrate energy storage with load-bearing capabilities, offering a promising solution to overcome current limitations.

Structural batteries differ fundamentally from conventional lithium-ion batteries in their design and functionality. State-of-the-art lithium-ion batteries typically use carbon-based anodes and cathodes such as lithium iron phosphate ($LiFePO_4$, LFP) or lithium nickel manganese cobalt oxide ($LiNiMnCoO_2$, NMC), along with liquid electrolytes housed in non-load-bearing casings. While multifunctional structural battery comprise constituents that simultaneously perform several functions, enabling mass reduction while preserving or even enhancing the intrinsic properties of individual components. For example, current studies indicate that replacing the roof of electric vehicles with structural batteries can significantly enhance the vehicle's driving range, while reducing its overall mass by

20% [4] [5]. In the aerospace industry, energy storage and weight distribution have long been challenges that need to be addressed and balanced. Structural batteries, with their unique combination of lightweight and load-bearing properties, have gradually emerged as a promising solution, making significant contributions to this field. By integrating energy storage into structural components like wings and fuselages, they reduce weight, improving overall aircraft performance. They also support hybrid-electric and fully electric propulsion systems, aiding the transition to carbon-neutral aircraft [6].

Globally, efforts are underway to mitigate and gradually prevent global warming. In Europe, the European Union has committed to reducing greenhouse gas emissions by 55% from 1990 levels by 2030 and achieving net-zero emissions by 2050 [7]. Transportation and industry are the primary sources of these emissions, making the widespread adoption of electric vehicles a crucial step toward meeting these climate targets. Electrification for decarbonization has emerged as the leading solution to the transportation sector's climate-related challenges. In the current state-of-the-art lithium-ion battery-powered vehicles, the integration of multifunctional material batteries presents a promising breakthrough. These advanced batteries not only help reduce the vehicle's weight but also enhance overall energy efficiency. By lowering weight and improving performance, such innovations have the potential to further protect the environment and contribute to a sustainable future.

Structural batteries have gained significant attention in both scientific research and industry due to their multifunctionality and numerous advantages. With characteristics such as mass-less and high energy density, it holds great promise compared to conventional lithium-ion batteries. The advent of structural batteries not only revolutionises energy storage but also has the potential to accelerate advancements across various industries. Through the integration of multifunctional structural power composites, the future of these technologies appears highly promising.

1.1 Battery concept

Batteries have become an essential part of daily life, providing convenience and driving significant advancements across various industries. A battery is a device that stores chemical energy and converts it into electrical energy through electrochemical reactions. It consists of several key components that work in unison to enable efficient energy storage and release. These components include the anode (negative electrode), cathode (positive electrode), electrolyte, and separator.

Lithium-ion batteries are one of the most popular batteries nowadays. But lithium was first discovered by Arfwedson [8] and Berzelius [9] by analysing petalite ore ($LiAlSi_4O_10$) in 1817, but it was not isolated until 1821 by Brande and Davy [10]. The rocking-chair battery concept was introduced in 1980, when Goodenough proposed the $LiCoO_2$ positive electrode. However, it required laboratory experiments to be scaled up for industrial application. This milestone was reached with the commercialisation of the $LiCoO_2$//hard-carbon battery by the Sony and Asahi Kasei teams, led by Nishi, in 1991. The rocking-chair concept later saw significant success in the Japanese battery industry, with notable contributions from Sony in 1985 [11] and Sanyo in 1988 [12].

Lithium-ion batteries can be composed of a variety of different positive and negative elec-

trode materials, resulting in different energy densities. Commonly used cathode materials include $LiCoO_2$ (cobalt oxide), which is widely adopted in consumer electronics due to its high energy density [13]; $LiFePO_4$ (lithium iron phosphate), known for its excellent thermal stability and long cycle life; and $LiMn_2O_4$ (lithium manganese oxide), which provides good safety and lower cost. On the anode side, graphite is the most commonly used material, appreciated for its good conductivity and relatively high energy density [13]. Research is also exploring hard carbon, particularly for sodium-ion batteries, due to its high cycling stability [14]. Furthermore, silicon-based materials are being investigated for their higher theoretical capacity compared to graphite, though challenges such as volume expansion and cracking during cycling still need to be addressed [15]. Lithium metal is another promising anode material for high-capacity batteries, but concerns regarding dendrite formation and safety remain significant barriers [16]. During the charge and discharge cycles, lithium ions are inserted and removed from the atomic layers of the active materials. Lithium-ion batteries (LIBs), as a widely adopted and commercially successful technology, offer high specific energy and energy density, making them ideal for applications where weight and volume are critical. However, despite their success, LIBs have nearly reached their performance limits in terms of capacity, power, and lifespan relative to their weight and cost, as indicated by ongoing demand analyses and research. One promising solution to overcome these limitations is the development of structural power composites, which have the potential to enhance battery performance.

1.2 Multifunctional structural power composite concept

There are two primary strategies for achieving multifunctionality in materials. The first involves integrating the desired functionality into a parent material, creating a multifunctional structure. The second approach views multifunctionality as a composite unit, where structural components work synergistically to deliver two or more functions simultaneously [17]. For example, polymer composites can withstand mechanical loads, store and deliver electrical energy, reduce mass, and maintain or even enhance the properties of individual components [17].

In the context of an electric vehicle (EV) battery pack, the lithium-ion battery in a Tesla Model S accounts for roughly 30% of the vehicle's total mass. If we simplify the vehicle into two main components—energy storage and exterior structure—it becomes clear that the exterior structure does not contribute to energy storage, nor does the energy storage system provide structural support. This separation increases the vehicle's total weight, lowering efficiency. However, using multifunctional structural composite materials can address both needs by providing structural integrity and energy storage, while also reducing overall mass, as shown in Figure 1.1 [18].

Figure 1.1: Structural power concept expressed in simple math relation [19].

1.3 Aims and limitations

Given the progress in the field and the increasing research demand, in this thesis work we aim to design and synthesize of lightweight, electromagnetically shielded composite materials by introducing high-throughput methods and magnetic field environments. Specifically, our focus will be on magnetic nanomaterials-graphene-carbon fiber composites, which are expected to significantly improve the deposition quality of active materials on CF. Simultaneously, the development of these shielded composite materials for structural batteries will be followed by rigorous testing of their EMI shielding efficiency in this way, seeking to advance the performance of structural batteries even further to meet the demands of this evolving world.

This study, while contributing valuable insights, has certain limitations. The scope of the research is constrained by time, resources, and current technological capabilities, which may affect the generalisation of the findings. Additionally, the experimental conditions may not fully replicate real-world scenarios, potentially limiting the practical applicability of the results. Despite these constraints, the outcomes provide a foundation for future research and development in the field.

1.4 Demarcations

This work primarily investigates the synthesis of structural battery cathode materials using the EPD method, structured in four key parts. First, various material recipes are tested on the original cathode formulation to evaluate their impact on subsequent battery performance. Second, a magnetic field is introduced during the EPD process to enhance the uniform deposition of the active material onto the CF. Third, EMI efficiency tests are conducted on the fabricated shielded composites. Fourth, a high-throughput approach is incorporated into the EPD process to accelerate the preparation and analysis of multifunctional composites. However, this study does not explore alternative battery active materials beyond LFP, nor does it investigate the optimal coating methods. Additionally, aspects such as life cycle assessment and the generation of comprehensive safety data are beyond the scope of this thesis. The primary focus of this paper is on material formulation, electrochemical performance improvements, and EMI efficiency, rather than a comprehensive evaluation of all potential factors affecting structural battery performance.

2

Theory

"Somewhere, something incredible is waiting to be known."

— *Carl Sagan*

As outlined in the background, the differences between structural batteries and lithium-ion batteries have been discussed. In this research, the process of developing structural batteries, ranging from the preparation of active materials to electrode fabrication and battery assembly, differs significantly from traditional lithium-ion battery manufacturing methods. This section will focus on introducing the base materials, preparation techniques, and testing methods essential to this research.

2.1 CF-based positive electrode

CF has emerged as a promising multifunctional material in LIB technology, offering a unique combination of mechanical strength and electrochemical performance. Its high tensile strength, low density, and excellent electrical conductivity make it an ideal candidate for advanced energy storage applications.

When utilised as a base electrode in LIBs, CF serves dual functions: as a current collector and as a structural reinforcement. This integration eliminates the need for traditional metal current collectors like aluminium and copper foils, thereby reducing the overall weight and complexity of the battery system. Additionally, the high surface area and tunable porosity of CF facilitate efficient ion transport and electron conduction, enhancing the charge/discharge rates and overall energy density of the battery. Recent studies have demonstrated the efficacy of CF-based electrodes in LIBs. For instance, LFP-coated CF electrodes have shown promising electrochemical performance, with specific capacities reaching up to 144 mAh g^{-1} at 0.1 C and maintaining 81.2% capacity retention after 300 cycles at 1.0 C. These results highlight the potential of CF as a substrate for active material deposition, ensuring uniform coating and strong adhesion, which are critical for long-term cycling stability [20].

Figure 2.1 provides a clear comparison between a conventional lithium-ion battery and a structural battery laminate, illustrating the key architectural differences. In traditional lithium-ion batteries (Figure 2.1a), energy storage components—such as active material particles, liquid electrolyte, and metallic current collectors (Al and Cu foils)—are distinct from the device's structural framework. These components add mass without contributing

to mechanical strength. In contrast, the structural battery design (Figure 2.1b) replaces these conventional elements with multifunctional materials. Notably, carbon fibres are employed not only as current collectors but also as active electrodes and structural reinforcements. The liquid electrolyte is replaced by SBE, which enables ionic transport while simultaneously bearing mechanical load. This integration eliminates the need for traditional metal foils and segregated structural casing, significantly reducing weight and improving system-level efficiency. The multifunctional use of carbon fibres within the laminate structure marks a pivotal advancement, enabling the simultaneous fulfilment of mechanical and electrochemical functions, and paving the way for lightweight, energy-dense systems ideal for aerospace, automotive, and wearable technologies.

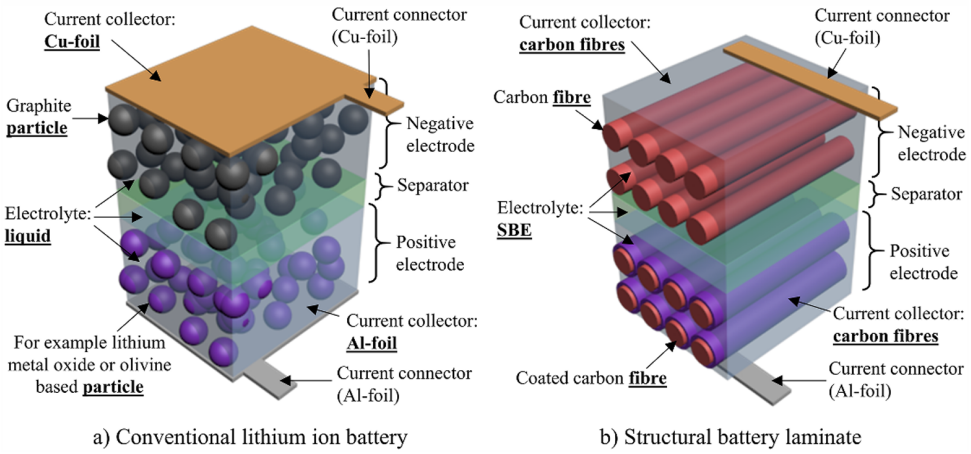

Figure 2.1: Schematic illustration of (a) a conventional lithium ion battery and (b) a laminated structural battery. SBE = Structural Battery Electrolyte. [21]

2.2 Electrophoretic deposition

In this study, electrophoretic deposition serves as the primary method for assembling a cathodic composite material directly onto the surface of carbon fibres. EPD is a well-developed, aqueous-based electrochemical deposition method in which suspended charged particles are deposited onto a surface with opposite charges under the application of a DC electric field. The EPD process primarily involves a power supply, an anode, a cathode, and a stable suspension. This process consists of two primary stages: electrophoresis, in which charged particles migrate toward the electrode under an applied electric field, and deposition, where these particles accumulate to form a uniform, adherent film on the substrate surface. Key suspension parameters that affect the coating morphology include particle size, liquid dielectric constant, electrical conductivity, medium viscosity, electrokinetic potential, and suspension stability. Additionally, factors such as deposition time, applied voltage, solid concentration in the suspension, and the substrate's conductivity play a significant role in influencing the process.

In this application, the process begins by immersing 3D-printed sample holders-integrated with CF and a platinum electrode—into a suspension containing LFP, CB, rGO, PDDA, and EtOH. This approach leverages the structural and conductive properties of CF, the high electrochemical stability and capacity of LFP, and the interconnected conductive network formed by CB and rGO. Through this method, active materials are directly de-

posited onto the CF substrate, allowing precise control over the coating process. The resulting composite structure exhibits enhanced electrical conductivity and increased surface area, which collectively support effective loading of active materials and promote efficient lithium-ion and electron transport during electrochemical cycling.

The preparation of a stable suspension is a crucial first step in the EPD process. Ethanol is selected as the solvent for dispersing LFP, CB, and rGO due to its low viscosity and relatively high dielectric constant, which aid in particle dispersion. To further stabilise the suspension, PDDA is introduced as a cationic polyelectrolyte. It imparts a positive surface charge to the particles, promoting uniform dispersion and preventing the aggregation of LFP and rGO, which are otherwise prone to clustering due to van der Waals forces and π–π stacking interactions, respectively [23] [36].

The incorporation of CB and rGO into the LFP matrix fulfils multiple roles. The addition of CB and rGO significantly improves the overall performance of the electrode, particularly by addressing the inherently low electronic conductivity of LFP (approximately 10^{-11} S/m). Incorporating an appropriate amount of CB enhances electrical conductivity and mechanical properties due to its high surface area, while also promoting a more uniform deposition layer on the CF substrate. However, excessive CB can negatively affect suspension stability, leading to poor dispersion and agglomeration within the deposited layer. The inclusion of rGO contributes to the formation of a three-dimensional conductive network across the deposition surface, enhancing both the uniformity and density of the coating. In addition, rGO improves the electrode's mechanical strength and flexibility. Its porous structure facilitates more efficient lithium-ion transport pathways, ultimately enhancing the rate performance of the electrode [23]. Optimising the concentration of LFP, CB, and rGO in the suspension is crucial for achieving balanced deposition.

The use of EPD to deposit LFP with CB, rGO, and PDDA onto CF substrates presents a promising strategy for fabricating high-performance Li-ion battery electrodes. By optimising suspension stability, EPD process parameters, and the concentration of carbon additives, it is possible to produce electrodes with improved electronic conductivity, mechanical integrity, and electrochemical performance. This approach offers considerable potential for advancing the development of next-generation energy storage systems.

Based on the aforementioned challenges associated with the EPD process, such as inconsistent deposition quality and uneven coating, a novel EPD strategy has been proposed to address these issues. This approach involves maintaining a magnetic field throughout both the deposition and subsequent drying processes. A magnetic field with a strength ranging from 0.2 to 1 Tesla will be applied. This magnetic field-assisted electrophoretic deposition (MAG-EPD) offers a green and sustainable approach with several advantages, including high efficiency, enhanced controllability, scalability, and cost-effectiveness. This technique anticipated outcome is that the deposited active materials will exhibit a higher degree of orientation, and the oriented deposits are expected to demonstrate a higher relative deposition density compared to randomly prepared coatings [24].

2.3 Electromagnetic interference

Electromagnetic interference (EMI) shielding refers to the creation of a barrier that effectively blocks the penetration of radio waves or microwave radiation, thereby protecting electronic devices or environments from interference [25]. EMI can result in data corruption, signal degradation, or total device failure, making effective shielding critical in modern electronic systems.

Carbon fibre (CF)-based materials have gained attention as effective EMI shielding materials due to their intrinsic electrical conductivity, high mechanical strength, and low density. The conductive nature of CF enables both reflection and absorption of electromagnetic waves, suppressing interference efficiently [26]. Moreover, CF's high aspect ratio and ability to form interconnected networks enhance its shielding effectiveness by facilitating multiple scattering and absorption mechanisms within the material [26].

Compared to conventional metal-based shields, CF composites offer several advantages, including lightweight structure, resistance to corrosion, and mechanical flexibility, which are particularly beneficial in aerospace, automotive, and wearable electronics applications. Additionally, CF-based materials can be processed into conformable and complex geometries without sacrificing shielding performance, enabling their use in integrated multifunctional systems.

In this work, a novel approach is proposed to fabricate high-efficiency EMI-shielded composite electrodes for structural batteries by incorporating both rGO and Fe_3O_4 into the EPD process. By adjusting the deposition parameters for each material, we aim to influence the microstructure of the active layer to improve EMI shielding performance. Furthermore, the EMI shielding effectiveness of the fabricated composites will be rigorously evaluated using VNA. This approach is expected to contribute to the advancement of structural battery composites with integrated EMI shielding capabilities.

Looking ahead, CF-based EMI shielding materials are expected to play an increasingly important role in next-generation electronic systems. Future developments will likely focus on enhancing multifunctionality, such as combining EMI shielding with thermal management, mechanical reinforcement, or structural energy storage. With the continued miniaturisation of devices and the rise in high-frequency electronics, the demand for lightweight, high-performance shielding materials like CF composites is anticipated to grow substantially [27].

2.4 Laminated SB architecture

The laminated structural battery architecture, illustrated in Figure 2.1, represents an advanced approach to integrating energy storage with structural integrity. In this design, the traditional components of a typical battery cell are reorganised into layers within a laminate structure. These layers include the active materials for both the positive and negative electrodes, separated by an insulating separator. Encasing these layers is a bicontinuous polymer known as the SBE, which not only facilitates ionic transport—vital for the battery's operation—but also enhances the mechanical load-bearing capacity of the structure. This dual-functionality of the SBE is crucial for applications where both

energy storage and structural strength are of equal importance, making it an ideal solution for industries requiring lightweight, high-performance materials.

2.5 Electrochemistry inside LIB cell

Electrochemical processes play a critical role in the functioning of LIBs by enabling the storage and release of energy. During discharge, lithium ions are released from the anode and travel through the electrolyte toward the cathode. During charging, this process is reversed, with lithium ions moving back from the cathode to the anode. Commercially available cathode materials include LFP, NMC, LCO, and LMO, while typical anode materials consist of graphite, silicon-graphite composites, and metal-based materials. As lithium ions move through the electrolyte, electrons flow through the external circuit, supplying electrical energy to power various devices. This movement of lithium ions between the anode and cathode facilitates the repeated cycling of the battery, enabling it to store and deliver energy.

In this study, only LFP and lithium metal were utilised as the cathode and anode active materials, respectively. Additionally, only half-cells were assembled to evaluate the electrochemical performance.

The electrochemical reactions occurring on the cathode and anode respectively are as follows:

$$\mathrm{LiMO_2} \rightleftharpoons \mathrm{Li_{1-x}MO_2} + x\mathrm{Li^+} + xe^- \tag{2.1}$$

$$\mathrm{Li} \rightleftharpoons \mathrm{Li^+} + e^- \tag{2.2}$$

Combining the equations above the full redox reaction is obtained:

$$\mathrm{LiMO_2} + x\mathrm{Li} \rightleftharpoons \mathrm{Li_{1-x}MO_2} + x\mathrm{Li} \tag{2.3}$$

In this context, $\mathrm{MO_2}$ represents a metal oxide, with Li serving as the negative electrode material. During lithiation, lithium ions from the cathode material (2.1) migrate to the anode to balance the potential difference in a closed circuit. Finally, the electrodes will be assembled into pouch cells for electrochemical performance testing of the battery. The prepared pouch battery cells will undergo a series of electrochemical tests to evaluate the performance of the fabricated cathode materials. Specifically, CV, galvanostatic charge-discharge and EIS will be employed to assess key performance such as capacity, charge-discharge efficiency, and electrochemical stability. These testing methods provide direct insights into the electrochemical behaviour of the cathode materials, offering critical data to guide future optimisation of fabrication processes and material design.

3

Materials and Methods

"Research is formalized curiosity. It is poking and prying with a purpose."

— Zora Neale Hurston

Following the theoretical background introduced in the previous section, this chapter presents the experimental methodology used to implement the proposed structural battery concept. It outlines the key materials, instruments, and procedures employed throughout the study. The research begins with the fabrication of carbon fibre-based cathode electrodes, emphasising the optimisation of deposition conditions. A high-throughput EPD method is then applied to accelerate and stabilise the coating process for preparing positive electrode composites. Finally, the fabricated electrodes are assembled into pouch cells, and their electrochemical performance is evaluated through systematic testing. This integrated workflow serves as the foundation for assessing the multifunctional properties of the developed structural battery system.

3.1 Materials

A detailed list of the materials employed in this study, including their sources and specifications, is provided in Table 3.1.

Table 3.1: Experimental Materials

Material Names	Suppliers
Torayca™ T800S 12K CFs	Toray
($LiFePO_4$) Lithium Iron Phosphate Nanopowder	Nanoshel
(CB) Carbon Black	Thermo scientific
(rGO, 95% Carbon content) Reduced Graphene Oxide	Layerone A/S
(PDDA) Poly(diallyldimethylammonium chloride)	Sigma
Fe_3O_4	Sigma
Molecular sieves	Sigma
Conductive Carbon Glue	Ted Pella
Conductive Sliver Paint	Ted Pella
(C_2H_5OH) Absolute Ethanol	Vwr
(CH_3COCH_3) Acetone	Vwr
(CH_2Cl_2) Dichloromethane	Vwr

3.2 Instruments

A summary of the experimental instruments utilised in this study is provided in Table 3.2.

Table 3.2: Experimental Instruments

Instruments	Suppliers
DC Power Supply	Keithley
Balance	Radwag
Vacuum Heat Sealer	Multivac
Glove Box	Vigor
Neware CT-4008-5V10mA 164 Battery Cycler	Neware
Oven	Heraeus
Vacuum Pump	BVV
Sonics VCX-750 Vibra-Cell Ultrasonic Liquid Processor	Sonics
Electrochemical Workstation	Biologic
Quanta 200 ESEM FEG	FEI
EM ACE600 Sputter Coater	Leica

3.3 Positive electrode fabrication

3.3.1 Sample preparation

To ensure reliability throughout the EPD process, the CF samples underwent a carefully designed preparation protocol. Initially, the carbon fibres were fixed onto a thin Teflon sheet and secured using PTFE tape to preserve their alignment during subsequent washing. The commercial carbon fibres, originally sized with a polymer sizing agent, were desized by immersion in either DCM or acetone for over 12 hours. This treatment improved the surface adhesion and uniformity of the subsequent coating, while also enhancing the intrinsic conductivity of the fibre surface. It is worth noting that, in this study, carbon fibres used for battery performance tests were desized, whereas those prepared for EMI shielding experiments retained their sizing layer.

Following the next step, the carbon fibres were repositioned onto 5 mm-thick Teflon substrates. The length and width of the fibres were controlled to approximately 40–45 mm and 15 mm, respectively, to facilitate subsequent pouch cell assembly and EMI shielding tests. Copper tape was applied at the top and Kapton tape at the bottom to maintain fibre orientation throughout the deposition. To quantify the amount of material deposited, the weights of all relevant components—including the Teflon substrate, copper tape, and Kapton tape—were measured prior to the experiment. The full assembly was then weighed at several stages: before deposition, immediately after EPD, and following drying at 70 °C. Additional mass measurements were taken while both tapes remained attached to the coated CF, enabling accurate determination of the carbon fibre mass, the deposited layer, and the active material. This systematic mass-tracking approach was essential for evaluating coating efficiency and active material loading on the electrode surface.

3.3.2 EPD recipe

The two EPD formulations were specifically applied to the preparation of structural battery cathodes and EMI shielding electrodes, respectively.

1. Structural battery cathode electrodes EPD recipe

   To prepare the cathode material using LFP as the active component, a formulation referred to as Recipe "2024" was employed. The process begins by thoroughly mixing LFP with CB using a mortar and pestle to ensure uniform dry blending. The resulting mixture is then dispersed in ethanol and subjected to 10 minutes of sonication. Subsequently, a pre-dissolved rGO solution in ethanol is added to the suspension, followed by another 10-minute sonication step to enhance dispersion. PDDA, dissolved in ethanol, is then introduced into the system, and any residual material from the weighing process is rinsed into the solution using additional ethanol. A final 20-minute sonication is carried out to ensure complete homogenization of the suspension prior to the EPD process.

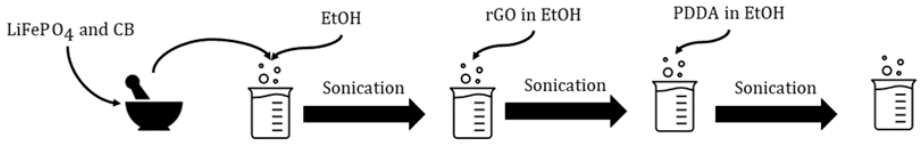

Figure 3.1: Schematic illustration of the EPD recipes used for structural battery cathode electrodes.

2. EMI shielding electrodes EPD recipe

   To fabricate the EMI shielding electrodes using Fe_3O_4 as the active ingredient, the initial step involved manually blending Fe_3O_4 and CB with a mortar and pestle to achieve a consistent dry mixture. This blend was then dispersed in ethanol and sonicated for 10 minutes to initiate dispersion. Afterwards, an ethanol based rGO solution was added to the suspension, followed by an additional 10-minute sonication to improve uniformity. PDDA, dissolved in ethanol, was subsequently introduced, and any remaining powder adhering to the weighing tools was washed into the solution using extra ethanol. To ensure a stable and homogeneous suspension suitable for deposition, the entire mixture underwent a final 20-minute sonication before the EPD process.

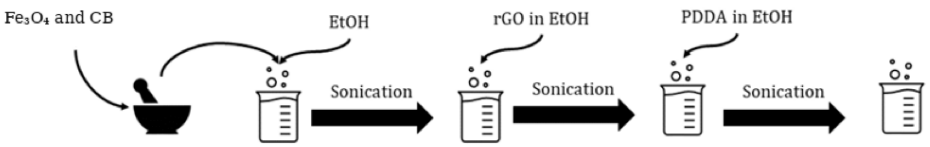

Figure 3.2: Schematic illustration of the EPD recipes used for EMI shielding electrodes.

It should be noted that that some suspensions were used immediately after the final sonica-

tion step, while others were stored overnight under continuous stirring in sealed containers to prevent solvent evaporation. Before proceeding with EPD, these stored suspensions were re-sonicated for 20 minutes to restore homogeneity. All sonication procedures were carried out using a tip sonicator (Sonics VCX-750 Vibra-Cell ultrasonic liquid processor) operated at 40% amplitude, corresponding to a tip excursion of 48µm.

3.3.3 EPD process

The EPD process was conducted through a series of controlled steps to ensure consistency across all samples:

The prepared carbon fibre electrode was connected to the negative terminal of the DC power supply, while the platinum counter electrode was connected to the positive terminal. Both electrodes were mounted in a custom-designed 3D-printed holder, which ensured a constant spacing of 2 cm between them throughout the deposition process.

The assembled electrodes were fully immersed in the EPD suspension, and a constant voltage was applied during the deposition process, with the current limited to a maximum of 0.6 A. When using the custom-designed two-electrode holder, 6 to 8 samples were typically prepared from a single batch of suspension. In addition, the three-electrode holder allowed for the preparation of 10 or more samples per batch. To maintain suspension stability and ensure uniform particle distribution, the solution was sonicated between each deposition cycle for a duration equal to half of the preceding EPD time. All sonication steps were performed using the Sonics VCX-750 Vibra-Cell ultrasonic liquid processor.

In total, 36 EPD batches were prepared during the course of this study, resulting in a total of 249 samples.

3.4 High-throughput method

High-throughput method (HTM) refer to a class of experimental strategies that aim to accelerate the discovery, screening, or optimisation of materials and processes by parallelising and automating the fabrication and testing steps. Originally popularised in pharmaceutical and catalyst research, high-throughput approaches are now increasingly adopted in materials science, especially in domains where time-consuming fabrication limits progress. By reducing the time, cost, and variability associated with traditional one-by-one experimentation, HTM enables the systematic evaluation of large parameter spaces, leading to faster iteration and data-driven decision making. When applied effectively, it can significantly enhance research efficiency and accelerate the transition from lab-scale discovery to practical implementation.

In this thesis, the high-throughput concept was applied to address the low efficiency of EPD processes, particularly in the context of preparing multiple carbon fibre cathodes for structural battery applications. The original EPD setup used a dual-electrode holder that allowed for the deposition of only one sample per run. Under standard settings (70 V for 20 minutes), preparing a batch of 10 samples would take over three hours, excluding drying and sonication steps.

To overcome this limitation, a series of deposition holders were designed and tested, in-

cluding four-electrode and three-electrode configurations. The four-electrode holder significantly increased deposition throughput but introduced instability and uneven current distribution. The three-electrode configuration, however, offered an optimal balance, enabling simultaneous deposition of multiple samples while maintaining coating quality and system stability.

In addition, deposition parameters were optimised for shorter cycle times (e.g., 80 V for 5 minutes), allowing up to 10 samples to be prepared in under one hour. This redesign, grounded in high-throughput principles, improved both experimental productivity and material comparability. As a result, this method provided a strong foundation for systematic studies involving different material recipes, including rGO content variations and EMI electrode development.

3.5 Structural battery cell fabrication

The assembly of structural battery cells involves a carefully controlled process carried out in an inert and moisture-free environment, specifically within a glove box maintained at oxygen and humidity levels below 1 ppm. The procedure utilises specialised materials, including glass substrates, pristine T800S carbon fibres as the negative electrode. A structural battery electrolyte is also employed. For the positive electrode, EPD-coated carbon fibre samples are used, integrating both electrochemical functionality and structural support.

3.5.1 Assembly process

During cell assembly, carbon fibres are attached to the current collectors using Pelco® Conductive Carbon Glue for the positive electrode. Prior to the final assembly of the pouch cell, the deposited electrodes are pre-packaged under vacuum following a defined procedure. This ensures that the prepared SBE can be thoroughly infused into the vacuum-sealed structure during the subsequent curing stage. The electrode stack is then constructed through the sequential layering of several materials: a release plastic film, a Freudenberg separator (from Freudenberg Performance Materials SE & Co.), a glass veil (6 g/m^2 , supplied by Technical Fibre Products Ltd.), and a textile mesh to ensure uniform pressure distribution. Tacky tape is applied along the perimeter of the stack to secure it to the glass substrate. Two rubber tubes, with felt wrapped around their ends, are inserted and extend outward for subsequent processing steps. The entire assembly is sealed with an outer plastic film and vacuum-packaged, typically containing electrodes sufficient for two half-cells. A vacuum pump is then used to check for any potential leakage and ensure the integrity of the seal. Once confirmed, the vacuum-sealed package is placed in a vacuum desiccator and dried in an oven for at least 12 hours. After the drying process is complete, the assembly is transferred into the glove box for SBE preparation, infusion and curing.

3.5.2 SBE preparation infusion and curing

The SBE mixture was prepared based on a previously reported procedure, with minor modifications. All steps were conducted inside an argon-filled glovebox under controlled

conditions ($H_2O < 1$ ppm, $O_2 < 1$ ppm) to ensure the moisture- and oxygen-sensitive components remained stable. First, a stock solution of 1.0 M liquid electrolyte was prepared by dissolving LiTFSI in a 50:50 wt.% mixture of ethylene carbonate (EC) and propylene carbonate (PC). This solution was then used to formulate the SBE by mixing it with the BPAMA monomer and 1wt.% of the thermal initiator AIBN (relative to the monomer content). The resulting mixture was homogenized using a vortex mixer and left to degas inside the glovebox before infusion.

For the infusion process, one rubber tube was connected to a syringe containing the prepared SBE mixture, while the other tube was sealed to prevent air ingress and premature curing. Once ready, the vacuum-sealed battery assembly was transferred out of the glovebox, and infusion was carried out at a controlled pressure of –0.6 bar. After reaching the target pressure, the inlet clamp was opened to initiate infusion. Upon completion, both clamps were closed—starting from the inlet side—and the sample was detached and transferred to a furnace for curing at 90 °C for 45 minutes. After curing, the sealed package was brought back into the glovebox, where the solidified electrode was retrieved and prepared for subsequent pouch cell assembly.

3.5.3 Half-cell preparation

Following the curing step, the cell is returned to the glovebox for final sealing. Each cell is placed into a pre-fabricated pouch bag, and the edges in contact with the current collectors are sealed using white tape and thermal tape to ensure electrical insulation.

The electrodes were then assembled in sequence, starting with the placement of the cathode electrode, which was pre-wetted with a small amount of LE. A Whatman separator was laid over the cathode to isolate it from the anode side and further wetted with 400 µL of LE. Four lithium metal sheets were subsequently positioned on top of the separator, evenly spaced to ensure full coverage of the cathode area. Finally, the open edge of the pouch was sealed using a vacuum heat sealer, completing the half-cell assembly.

3.6 Electrochemical performance evaluation

The assembled structural battery cells were comprehensively evaluated using a Neware CT-4008-5V10mA164 battery cycler, which enables precise control and real-time data acquisition. The electrochemical characterisation included CV, GCD, and EIS.

Due to time constraints, this study focused exclusively on the fabrication and testing of half-cells. Following assembly, the half-cells were immediately subjected to a series of electrochemical characterisations, including open-circuit voltage (OCV), CV and EIS.

Subsequently, galvanostatic charge-discharge cycling was carried out at a range of C-rates to evaluate the electrochemical performance of the electrodes. The applied current rates were calculated based on the theoretical capacity of the LFP-coated cathode. The cycling protocol involved ten full charge/discharge cycles at C/20, followed by five cycles each at C/10, C/5, C/2, and 1C. A rest period of two minutes was introduced between cycles to allow ionic concentration gradients within the cell to equilibrate.

In total, four structural battery cells with different configurations were fabricated and

evaluated to assess their electrochemical behaviour and multifunctional performance.

3.7 Material characterisation

3.7.1 Scanning Electron Microscopy

SEM was employed as a key technique to investigate the microstructure and surface morphology of the materials at high magnification. This method was especially important for analysing both the surface characteristics and cross-sectional architecture of the electrode materials used in the structural battery cells.

3.7.2 Sample Preparation

For SEM analysis, a FEI Quanta 200 ESEM FEG instrument was used. Coated carbon fibre samples were carefully trimmed to the appropriate size using sharp scissors and subsequently handled with tweezers. The prepared samples were directly mounted onto aluminium stubs using conductive carbon tape. To improve surface conductivity and enhance imaging quality, a thin gold layer—approximately 5 nm in thickness—was applied via sputter coating using the Leica EM ACE600 system. This conductive coating effectively minimised charging effects and contributed to improved clarity and resolution in the SEM images.

3.7.3 Imaging and Analysis

SEM imaging enabled the acquisition of high-resolution surface and cross-sectional views of the coated samples. Through high-magnification observations, the uniformity of the LFP and carbonaceous material coatings on the carbon fibres was closely examined. This analysis provided valuable insights into microstructural consistency and helped identify potential defects that could influence the electrochemical performance of the battery cells.

Cross-sectional imaging further allowed for the measurement of coating thickness and evaluation of the interface between the active material and the carbon fibre substrate. These observations are essential for understanding how the structural characteristics of the coating influence the electrochemical behaviour of the electrodes.

4

Results

"If we knew what we were doing, it would not be called research, would it?"

— Albert Einstein

This study focuses on four key research directions aimed at improving the performance and scalability of structural battery electrodes. First, building on the EPD recipe developed by Dr. Richa Chaudhary in 2024, we introduced a magnetic field during deposition to enhance coating uniformity and consistency across different material combinations—results that proved promising. Second, to address the growing need for efficient fabrication, we integrated a high-throughput method by redesigning the EPD sample holder and refining the preparation process, which significantly accelerated electrode production. Third, to expand the applicability of EPD beyond structural batteries, we employed Fe_3O_4 as an active material for EMI shielding electrodes, adapting the process to suit its characteristics and confirming EPD's versatility. Lastly, using the original LFP-based recipe, we systematically varied rGO content and assessed its influence on electrochemical performance through half-cell testing, providing insights into the role of conductive additives in multifunctional electrode systems.

Following the Materials and Methods chapter, we now move into the Results and Discussion section, where the experimental findings are critically examined. This chapter explores both the anticipated results and the unforeseen outcomes that emerged during the investigation. Through detailed analysis, we aim to interpret the underlying mechanisms and correlations revealed by the data, while also addressing experimental uncertainties and variations that may influence the performance and behaviour of the structural battery system.

This study is structured around four key areas of investigation, each addressing a specific challenge or opportunity in the development of structural battery electrodes.

The first part builds upon the EPD formulation introduced by Dr. Richa Chaudhary in 2024. To enhance the deposition quality and consistency of structural battery cathode electrodes, we proposed the introduction of an external magnetic field during the EPD process. Under various magnetic field conditions, multiple material combinations with different component ratios were tested. The results were highly encouraging, demonstrating improved coating uniformity and deposition control, offering a novel route to engineer high-quality structural electrodes.

The second focus addresses the growing demand for faster and more scalable structural battery electrode fabrication. As the original preparation workflow became increasingly insufficient to support the pace of experimental development, we integrated a high-throughput strategy into the electrode manufacturing process. This was achieved by redesigning the sample holder used during EPD and refining both the deposition and post-processing steps. These modifications significantly accelerated electrode production, enabling rapid experimental advancement and laying a practical foundation for the future industrial-scale commercialisation of structural battery technology.

In the third part of the study, we explored the extension of EPD applicability to new materials within the context of EMI shielding electrodes. Motivated by the dual objectives of addressing EMI functionality and broadening the use of EPD, Fe_3O_4 was selected as an alternative active material for shielded electrode fabrication. The deposition process was adapted and optimised to accommodate the distinct characteristics of Fe_3O_4, demonstrating EPD's versatility beyond traditional structural battery applications and validating its potential in multifunctional material systems.

Finally, the fourth component returned to the original EPD recipe developed by Dr. Richa Chaudhary, combined with the high-throughput fabrication method. In this phase, structural battery cathodes based on LFP as the active material were prepared. Using the original formulation as a baseline, we systematically varied the rGO content to investigate its influence on electrochemical performance. Half-cell configurations were fabricated and tested to evaluate changes in conductivity, stability, and capacity retention. The results provide insight into the impact of conductive additives on electrode behaviour and offer valuable guidance for future material optimisation in multifunctional energy storage systems.

4.1 Desizing Method

Desizing is a crucial step in preparing carbon fibres for subsequent surface treatments and coatings, particularly in processes such as EPD. The commercial sizing layer, though beneficial for handling and processing, often inhibits adhesion and uniform deposition of active materials. In this study, T800S carbon fibres were desized by immersion in DCM for over 12 hours to ensure thorough removal of the surface sizing.

As shown in Figure 4.1, SEM images at low magnification reveal a noticeable transformation in surface morphology following DCM treatment. Compared to the sized fibres, the desized carbon fibres display a smoother and more uniform surface texture. This smoother surface promotes more consistent and conformal deposition during the EPD process, improving the adhesion and coverage of the active material layer.

In the later stages of this research, acetone was also evaluated as an alternative desizing solvent. It was observed that acetone produced a similar desizing effect, offering a practical and less hazardous substitute to DCM. The cleaned carbon fibres, prepared through either method, were subsequently used as cathode substrates in the fabrication of structural battery electrodes.

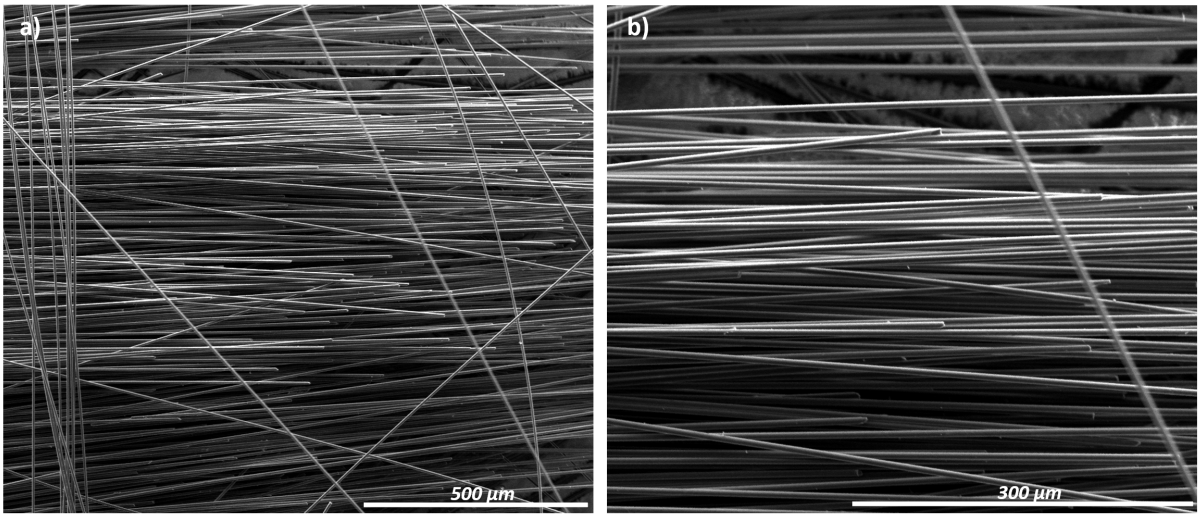

Figure 4.1: SEM images of desized T800S carbon fibres after reflux in DCM for over 12 hours

4.2 EPD: Positive Electrodes Manufacturing

Building upon the original EPD method, this study focused on the systematic development of a more effective approach for manufacturing positive electrodes. Modifications were made across multiple aspects of the process, including equipment configuration, deposition parameters, and material formulation. Key improvements involved the introduction of a controlled magnetic field during deposition, the redesign of the sample holder to enable higher throughput and better stability, and the adjustment of material compositions to enhance coating quality and uniformity. The following results highlight the effects of these changes on the performance and morphology of the fabricated electrodes.

4.2.1 Magnetic Field-Assisted EPD

T800S carbon fibres desized with DCM were successfully functionalised with a $LiFePO_4$/ CB/ rGO coating via EPD. Using the previously described EPD recipe without magnetic assistance, the fabricated electrodes were assembled into half-cells and subjected to electrochemical testing. The electrochemical testing revealed limited performance under the initial conditions. According to the findings reported by Nduka et al, applying a magnetic field during the drying process can significantly enhance the performance of LFP cathodes by improving electrochemical properties, reducing polarisation, and facilitating lithium-ion diffusion[28].

Inspired by previous findings on magnetic field-assisted electrode preparation, and as shown in Figure 4.2, the present study introduced a magnetic field at two critical stages of the EPD process. First, a magnet was positioned beside the working electrode (carbon fibre side) during the final 5 minutes of deposition. Second, immediately after deposition, the freshly coated samples were placed on a magnet for 20 minutes during the drying stage. This dual application of magnetic fields aimed to improve the uniformity and electrochemical functionality of the resulting cathode coatings.

Figure 4.2: EPD Magnet Set-up: A small magnet placed adjacent to the working electrode during deposition to aid in magnetic alignment. After the deposition, the sample was dried on a large magnet for 20 minutes.

To evaluate the influence of magnetic fields on EPD deposition efficiency, a series of experiments were conducted under fixed deposition conditions (80 V, 5 min), while varying the mass ratios of LFP, CB, and rGO. The primary variable was the presence or absence of a magnetic field during the final stage of deposition. As shown in Tables 4.1 to 4.3, three different material compositions were tested: 450:25:25, 425:25:50, and 400:50:50, respectively.

In both Table 4.1 and Table 4.2, the results indicate that the inclusion of a magnetic field leads to a noticeable increase in the average deposited LFP mass. For instance, under the 450:25:25 composition, the deposition mass increased from an average of 22.71 mg (without magnet) to 23.06 mg (with magnet), while for the 425:25:50 composition, the increase was more pronounced—from 25.73 mg to 30.72 mg. These findings suggest that the magnetic field enhances the consistency and efficiency of particle transport and deposition onto the carbon fibre substrate. Correspondingly, the average areal loading of the active material under magnetic influence was consistently in the range of 3.5–5.5 mg/cm^2, $indicating stable deposition across different formulations$.

However, in Table 4.3, corresponding to the 400:50:50 composition, the opposite trend is observed—the average deposition mass without a magnetic field (30.58 mg) exceeded that with a magnetic field (28.24 mg). This deviation may be attributed to the significantly increased concentration of carbon black and rGO in this formulation, which could alter the suspension's magnetic responsiveness and increase interparticle repulsion or agglomeration under the magnetic field. According to Ma Z., high concentrations of CB and rGO are prone to agglomeration in solution, which decreases particle dispersion and negatively affects the uniformity and compactness of the deposited film[29]. The dense particle loading might also affect mobility and alignment during deposition, thereby reducing the overall deposition efficiency when the magnetic field is applied.

Table 4.1: Comparison of LFP Deposition Mass With and Without Magnetic Field (KK53–57: No Mag, KK58–62: Mag)

Materials	LFP 450 CB 25 rGO 25	**Active material (LFP) [mg]**	
Setting	80V 5min	**Without Magnet**	**With Magnet**
1		18.20	25.93
2		18.27	20.69
3		25.69	28.42
4		28.97	19.44
5		22.45	20.81
Average		**22.71**	**23.06**

Table 4.2: Comparison of LFP Deposition Mass With and Without Magnetic Field (KK68-72: No Mag, KK83-87: Mag)

Materials	LFP 425 CB 25 rGO 50	**Active material (LFP) [mg]**	
Setting	80V 5min	**Without Magnet**	**With Magnet**
1		27.03	28.35
2		27.20	36.97
3		24.17	28.60
4		26.44	32.39
5		23.83	27.30
Average		**25.73**	**30.72**

Table 4.3: Comparison of LFP Deposition Mass With and Without Magnetic Field (KK73-77: No Mag, KK78-82: Mag

Materials	LFP 400 CB 50 rGO 50	**Active material (LFP) [mg]**	
Setting	80V 5min	**Without Magnet**	**With Magnet**
1		31.54	34.05
2		31.92	27.35
3		31.33	30.34
4		28.17	28.00
5		29.93	21.45
Average		**30.58**	**28.24**

The SEM analysis was conducted to further investigate the influence of magnetic field application on the deposition quality and surface morphology of EPD-coated samples. As shown in Figure 4.3, secondary electron images at various magnifications are presented. Figures 4.3a,b and c correspond to sample KK57, deposited without a magnetic field, while

Figures 4.3d, e, and f represent sample KK62, deposited with a magnetic field. At low magnification (Figures 4.3a and 4.3d), notable differences in surface morphology can be observed. The sample without magnetic assistance (Figure 4.3a) exhibits uneven particle distribution, with localised agglomeration forming "blocky" clusters. In contrast, the magnetically assisted sample (Figure 4.3d) shows a more continuous and dense deposition layer, with reduced agglomeration and a more uniform, directionally textured coating. At 1000× magnification (Figures 4.3b and 4.3e), these trends become more pronounced. The KK57 sample reveals a rough surface with inconsistent coverage—large areas of exposed carbon fibre and visible gaps are present. In comparison, the KK62 sample demonstrates a more homogeneous coating across the fibre surface, with finer particles, denser structure, and improved thickness uniformity. At higher magnification (2000×, Figures 4.3c and 4.3f), particle agglomeration becomes more evident in both samples. However, KK62 still exhibits smaller, more interconnected particles, suggesting improved microstructural continuity.

Overall, the SEM observations confirm that magnetic field application during EPD leads to enhanced deposition quality. The KK62 sample exhibits a denser and more uniform coating, smaller particle size, and reduced agglomeration—features typically associated with improved electronic contact, better mechanical stability, and potentially enhanced ion transport properties. These morphological improvements indicate that the integration of a magnetic field into the EPD process can be an effective strategy for producing higher-quality electrode coatings.

Although these structural advantages suggest the potential for improved electrochemical performance, further validation through full cell assembly and electrochemical tests such as OCV, CV, and EIS is necessary. Due to the limited scope and time frame of this study, such evaluations were not conducted.

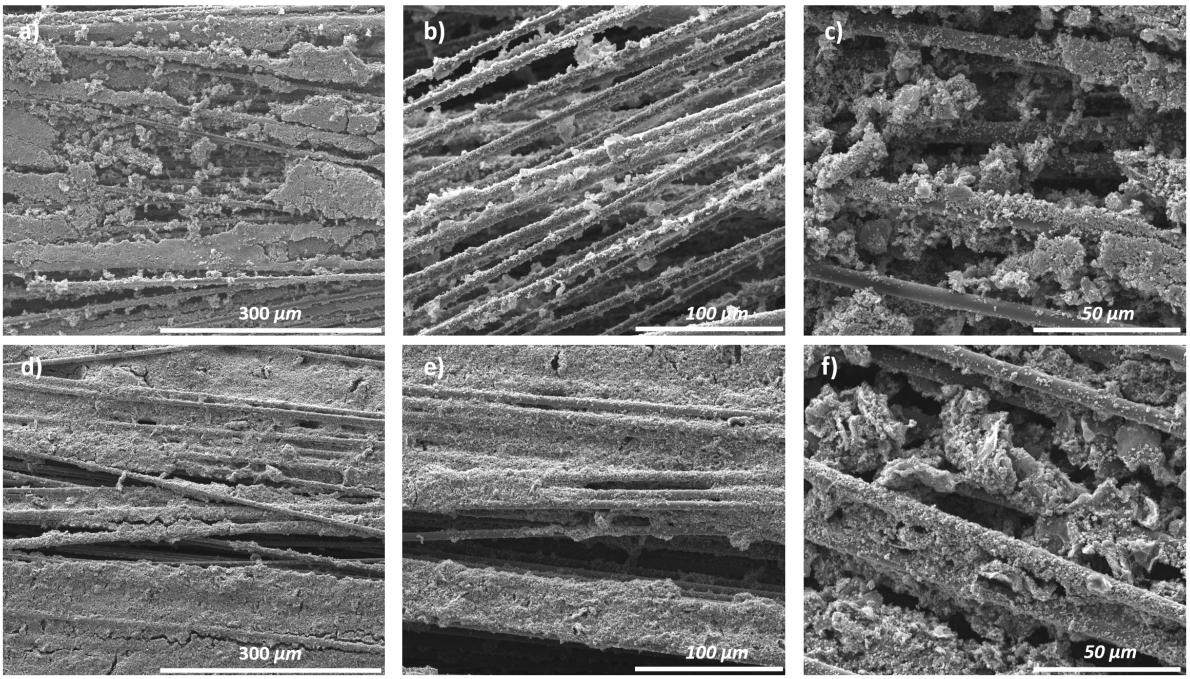

Figure 4.3: SEM images under 500x, 1000x, 2000x magnification.(a–c): KK57 (without magnetic field),(d–f): KK62 (with magnetic field).

4.2.2 Integration of High-Throughput Methods for Electrode Fabrication

High-throughput method is defined as the miniaturisation and parallelisation of experimental conditions, enabling a large number of tests to be performed simultaneously with minimal material consumption [30]. This approach has gained increasing traction in both industry and academia, particularly in areas of materials discovery, optimisation, and device fabrication [31].

In this study, the fabrication of cathode electrodes for structural batteries has long been hindered by low production efficiency and time-consuming procedures. These limitations not only slow the pace of material screening and characterisation, but also present significant challenges in scaling up structural battery technologies toward commercial viability. To address these issues, a high-throughput fabrication strategy was introduced in this work, aiming to accelerate the electrode preparation process while maintaining material quality and consistency.

The baseline approach is derived from procedures developed by Chaudhary et al. [32], which utilizes a dual-electrode sample holder system—comprising one working electrode (carbon fibre) and one counter electrode (platinum), as shown in Figure 4.4. Under standard conditions (70 V for 20 minutes per sample), the preparation of 10 samples would require approximately 200 minutes, excluding time allocated for sonication and drying. This limited throughput prompted the redesign of the electrode holder system to increase parallel capacity.

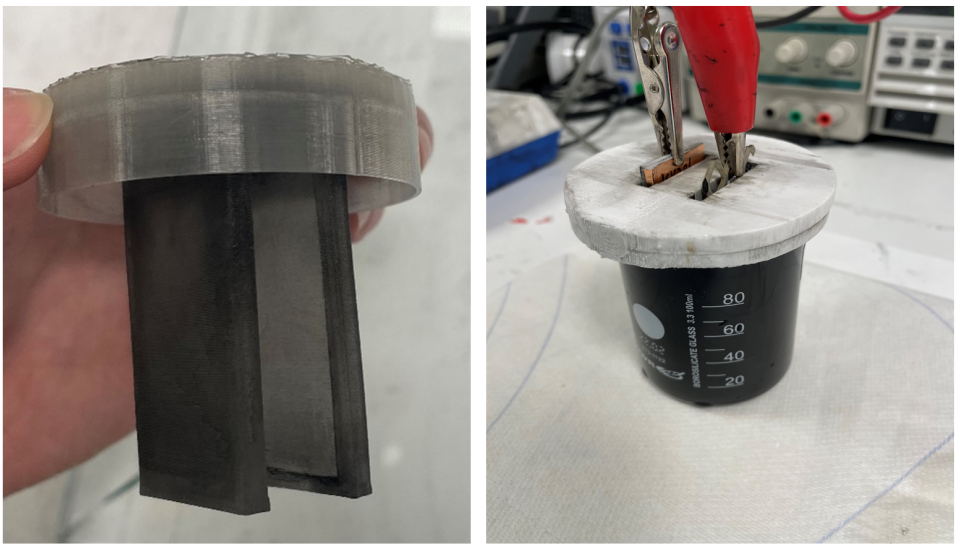

Figure 4.4: Dual-electrode holder

In the initial redesign, a four-electrode configuration was developed (Figure 4.5), incorporating two working electrodes and two counter electrodes. Alongside this hardware upgrade, the deposition parameters were adjusted to 80 V for 5 minutes per sample. This modification successfully reduced the total deposition time for 10 samples from 200 minutes to just 50 minutes—a 75% increase in fabrication efficiency.

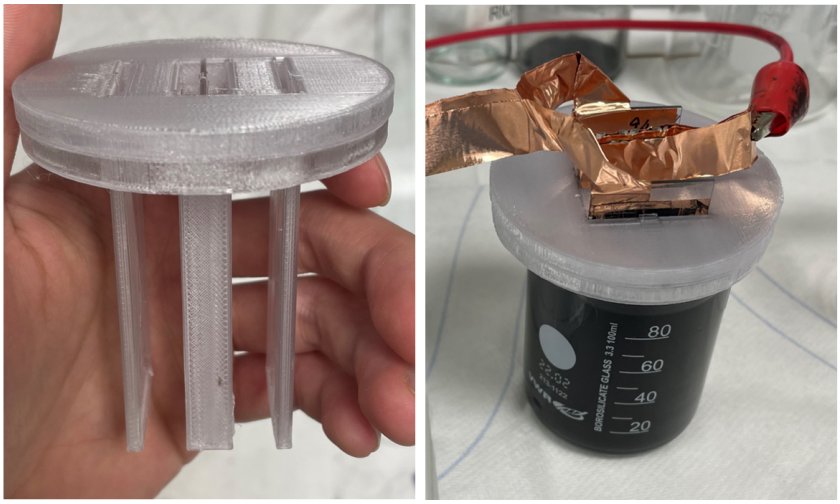

Figure 4.5: Four-electrode holder

However, several issues arose during this high-throughput implementation. Instabilities such as overheating of the suspension and large, unstable current fluctuations during deposition were observed. These problems were reflected in the deposition outcomes, as summarised in Table 4.4. The average loading mass from the four-electrode setup was notably lower than that obtained with the dual-electrode system, and the uniformity and quality of the deposited films were less reliable. These results suggested that while the four-electrode configuration improved speed, it compromised control and coating consistency.

To resolve these challenges, the system was further refined into a three-electrode configuration (Figure 4.5), consisting of two working electrodes and one counter electrode. This reduction in counter-electrode complexity helped to stabilise the deposition environment without sacrificing efficiency. As evidenced by the improved deposition uniformity and average mass loading shown in Table 4.4, the three-electrode system offered a balance between efficiency and quality. The resulting electrodes exhibited more stable loading values and superior film uniformity compared to the four-electrode setup, confirming the effectiveness of this optimisation.

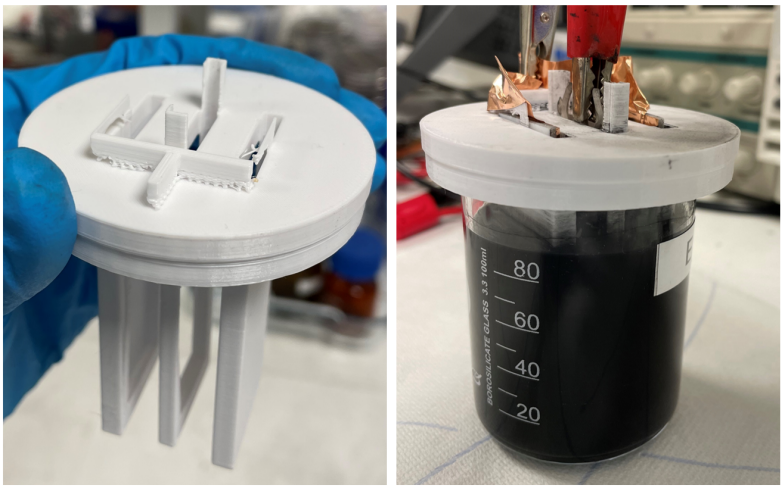

Figure 4.6: Three-electrode holder

Table 4.4: Comparison of deposited active material loading using different electrode holders.

Holders	**Dual-electrode holder**	**Four-electrode holder**	**Three-electrode holder**
Samples	**Active material (LFP) [mg]**		
1	26.84	8.60	34.36
2	30.97	12.75	19.24
3	34.76	13.54	38.22
4	21.55	14.58	26.81
5	20.51	13.52	31.09
6	26.32	13.43	24.71
7	—	—	20.27
8	—	—	17.04
Average	**26.83**	**12.74**	**26.47**

The integration of high-throughput methodology into EPD-based cathode fabrication significantly accelerated the process while maintaining—or in the case of the optimised setup, even improving—material quality. This approach provides a viable foundation for scaling up structural battery electrode production in future industrial applications.

4.2.3 Expanding EPD Applicability: EMI Shielding Electrode Fabrication

This study also explored the potential of applying EPD to areas beyond structural batteries, particularly in the field of EMI shielding. As outlined in the theoretical background, CFs inherently exhibit electrical conductivity, low density, and high mechanical strength—properties that make them ideal candidates for EMI shielding materials. With the rising demand for lightweight, multifunctional shielding solutions in aerospace, automotive, and consumer electronics, the integration of EMI shielding capability within structural battery components presents an attractive opportunity for material and system-level innovation.

Motivated by these material properties and the increasing significance of EMI mitigation in complex electronic environments, this study explored the use of EPD for fabricating shielded electrodes. Specifically, the aim was to extend the versatility of the EPD process by demonstrating its applicability in producing functional composites for EMI applications. In contrast to traditional metal-based shields, CF composites offer advantages such as corrosion resistance, ease of integration, and conformability to various shapes—qualities that align well with modern design demands.

In selecting active materials for EMI shielding, Fe_3O_4 was chosen as a key component due to its unique combination of magnetic and dielectric loss mechanisms. Fe_3O_4 nanoparticles are known to exhibit excellent EMI shielding performance through absorption-dominated pathways, attributed to their inherent magnetic permeability and the ability to interact with electromagnetic waves across a broad frequency spectrum. Literature supports the use of Fe_3O_4 in EMI shielding composites, demonstrating that their inclusion enhances attenuation efficiency and overall shielding effectiveness. For example, Saini et al. reported that Fe_3O_4, when embedded into conductive matrices, significantly improved EMI

shielding effectiveness by introducing both reflection and absorption losses [27]. Similarly, Bayat et al. confirmed that Fe_3O_4 incorporated into carbon nanofibre composites enhanced shielding performance primarily through absorption mechanisms, demonstrating its suitability for lightweight EMI applications [33]. Yu et al. also demonstrated that rGO/Fe_3O_4 hybrids embedded in carbon foams provided highly efficient EMI shielding while maintaining structural robustness, making them promising for multifunctional applications [34]. Furthermore, Sparavigna highlighted the potential of Fe_3O_4 nanoparticles for EMI shielding when integrated into conductive polymer matrices, due to their strong magnetic permeability and dual loss mechanism capability [35]. But, research specifically focusing on the integration of Fe_3O_4 with carbon fibre substrates for EMI shielding remains relatively limited.

To demonstrate the feasibility of this approach, Fe_3O_4 was used in combination with CB and rGO as the active deposition constituents. The formulation and EPD process were carefully adjusted to accommodate Fe_3O_4 compared to LFP. To achieve an EMI electrode with theoretically sufficient shielding performance, the ideal areal loading on the carbon fibre substrate is estimated to be approximately 4–6 mg/cm². Initial depositions were performed using the standard LFP-based EPD recipe to evaluate baseline performance. However, the resulting electrodes showed lower-than-expected loading values, typically ranging between 2–4 mg/cm², indicating a clear gap from the desired target. To address this, the experimental strategy was revised: after completing one full EPD deposition processes—including the final drying stage—the same suspension was freshly prepared at the same concentration, and a second deposition was conducted directly on the coated samples. As shown in Table 4.5, three batches of deposition notably improved the areal mass loading, with most samples reaching the desired range of 4–6 mg/cm². The successful deposition of Fe_3O_4-based composites via EPD not only validated the flexibility of the technique but also emphasised its adaptability to other functional domains.

Table 4.5: Deposition mass of Fe_3O_4-based active materials.

Materials	Fe_3O_4 450 CB 25 rGO 25	**Active materials (Fe_3O_4) [mg]**		
Setting	80V 5min			
1		34.40	42.83	57.16
2		33.23	31.93	46.04
3		60.92	38.87	43.20
4		55.68	30.64	35.93
5		42.87	31.95	42.11
6		40.17	32.86	33.30
7		32.60	26.62	32.73
8		39.09	26.30	29.25
9		—	23.72	23.56
10		—	30.33	22.44
Average		**42.37**	**31.61**	**36.57**

By incorporating EMI shielding considerations into the broader context of structural battery development, this study explored the potential of EPD as a method that connects

electrochemical and electromagnetic functionalities. The dual-role capacity of CF-based materials—as both energy storage elements and EMI shielding components—demonstrates the promise of this integrable behaviour. However, due to time limitations, EMI performance testing was not carried out in this work. To further evaluate the effectiveness of Fe_3O_4-coated carbon fibres for EMI applications, future studies could include shielding effectiveness measurements using VNA across relevant frequency ranges. Such testing would help validate the feasibility of this multifunctional design.

4.3 Electrochemical Performance

Electrochemical performance is a key indicator for evaluating the effectiveness of electrode materials in structural batteries. As structural batteries are designed to fulfill both mechanical and electrochemical functions, a comprehensive understanding of their electrochemical behaviour is essential to advancing their development. Assessing parameters such as capacity, internal resistance, and cycling stability provides valuable insight into material performance and guides further optimisation for practical applications. In this study, the electrochemical performance of LFP-coated carbon fibre cathodes—prepared without magnetic field assistance—was systematically investigated with a focus on varying rGO content (25 mg, 50 mg, and 75 mg). By tuning the amount of rGO in the electrode composition, the aim was to examine its influence on the overall electrochemical behavior of the structural cathodes. Following the assembly of the pouch cells, a series of electrochemical tests were conducted in the order of OCV, EIS, CV, a second EIS measurement and GCD. The dual EIS tests—performed before and after the CV—were intended to capture any changes in internal resistance caused by the electrochemical cycling, thus providing additional insight into the stability and interface behaviour of the electrodes under operational conditions.

In total, four cathode electrodes were evaluated in this study, namely KK58, KK66, KK71, and KK93, with their specific material compositions detailed in Table 4.6. Among these samples, several CV, EIS, and GCD measurements yielded incomplete or unusable data due to experimental inconsistencies, such as unstable contacts, unexpected electrode degradation, or poor electrolyte wetting. As a result, only the most representative and technically sound results are presented in the following figures to ensure clarity and reliability of the analysis. It is important to note that minor fabrication or handling issues can significantly affect electrochemical performance. Therefore, to avoid misleading conclusions, more systematic battery-level testing and repeated trials should be conducted in future work. These additional efforts will help minimise the influence of uncontrolled variables and improve the robustness and reproducibility of the data.

Table 4.6: Composition and deposition results of KK58, KK66, KK71 and KK93.

Materials	KK58	KK66	KK71	KK93
LFP	450	400	425	400
CB	25	25	25	75
rGO	**25**	**75**	**50**	**25**
PDDA	450	400	425	400
EtOH	100	100	100	100
Active material (LFP) [mg]	25.93	25.43	26.44	26.32
Active material (LFP) [mg/cm²]	3.86	3.85	3.76	4.28

4.3.1 Cyclic Voltammetry

Cyclic voltammetry (CV) is a fundamental electrochemical technique used to evaluate the redox reversibility and reaction kinetics of electrode materials. By analysing the position, shape, and symmetry of the anodic and cathodic peaks, researchers can assess the charge storage behaviour, conductivity, and structural stability of the electrodes. In the context of lithium-ion batteries, CV provides crucial insights into the intercalation and deintercalation processes of lithium ions, enabling the evaluation of active material utilization and electrochemical reversibility.

As shown in Figure 4.7, both the KK71 (a) and KK93 (b) electrodes display highly symmetrical redox peaks with well-overlapped profiles, indicating excellent electrochemical reversibility and structural stability during cycling. For the KK71 electrode (Figure 4.7a), the cathodic peak appears at 3.29V with a current of −0.10A, while the anodic peak is located at 3.61V with a current of 0.12A. The resulting peak potential separation (ΔE_p) is approximately 0.32 V, reflecting a fast charge transfer process and low electrode polarisation. In contrast, the KK93 electrode (Figure 4.7b) exhibits a cathodic peak at 3.11V (−0.07A) and an anodic peak at 3.76V (0.08A), resulting in a significantly larger ΔE_p of 0.65V. This broader separation suggests a slower electron transfer rate and higher internal resistance. Furthermore, the lower peak currents in KK93 indicate fewer electrochemically active sites and reduced ion mobility. Although KK93 exhibits a slightly higher redox potential, which may reflect a stronger thermodynamic driving force for Li^+ intercalation, its kinetic limitations dominate, leading to lower overall performance. The overall internal resistance of KK71 is lower than that of KK93, which may be attributed to the reduction of carbon black and the increased content of rGO. Excessive carbon black can lead to poor dispersion during initial deposition, thereby compromising coating uniformity. In contrast, an appropriate increase in rGO content improves suspension homogeneity and coating uniformity, while its porous structure provides enhanced pathways for Li^+ transport, effectively reducing the overall structural resistance and improving charge transport efficiency.

Control experiments in previous work underscore the critical role of both conductive additives. Without carbon black, the CV curve became nearly flat, indicating severely limited conductivity due to the inherently poor electron transport in LFP. Excluding graphene oxide led to broader and weaker redox peaks, suggesting hindered electron mobility and slower reaction kinetics [36]. These results highlight the synergistic effect of combining CB and rGO, and underscore the importance of precisely optimising their ratio to enhance

the electrochemical performance of EPD-derived electrodes.

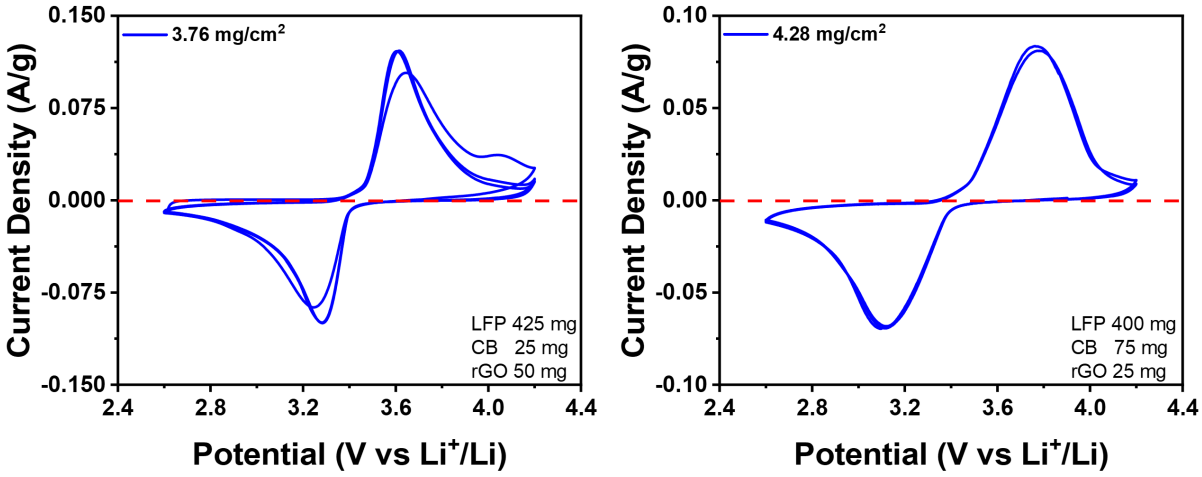

Figure 4.7: a) KK71 CV plot. b) KK93 CV plot.

4.3.2 Electrochemical Impedance Spectroscopy

EIS is a powerful technique used to evaluate the internal resistance characteristics of battery cells and to gain insight into interfacial and charge transport processes. By applying a small AC voltage over a range of frequencies, EIS measures how the cell responds to different types of electrochemical interactions. The resulting impedance spectrum can be used to identify and quantify different resistance components within the cell. These typically include the bulk resistance (R_s), which reflects the ionic resistance of the electrolyte; the charge transfer resistance (R_{ct}), which represents the resistance at the electrode–electrolyte interface; and the Warburg impedance (Z_w), which is associated with lithium-ion diffusion in the electrode materials. Together, these parameters provide a detailed view of the cell's internal kinetics and are essential for assessing electrode performance and stability.

As shown in Figure 4.8a, for the KK71 electrode, R_s decreased from 14.56 Ω (Before CV) to 9.06 Ω (After CV), indicating a modest enhancement in ionic conductivity, potentially due to improved electrolyte infiltration into the porous electrode structure after electrochemical activation. In addition, R_{ct} exhibited a significant drop from 35.24 Ω to 20.19 Ω, suggesting faster charge transfer kinetics, likely facilitated by increased electrochemically active surface area or enhanced electrode–electrolyte contact. Notably, the low-frequency tail became less steeper after CV, implying an increase in Warburg impedance (Z_w), which reflects high resistance in lithium-ion diffusion through the electrode matrix.

In contrast, the KK93 electrode showed a decrease in R_s from 28.65 Ω to 9.98 Ω, indicating a substantial reduction in ionic resistance, which may be attributed to better electrolyte wetting or redistribution of conductive additives during CV cycling. However, R_{ct} increased slightly from 90.06 Ω to 109.25 Ω, pointing to a deterioration in charge transfer efficiency, possibly due to heterogeneous particle distribution, local agglomeration, or partial blockage of electroactive sites. Interestingly, the slope of the diffusion tail in the low-frequency region became less steep after CV, suggesting an increase in Warburg impedance (Z_w), and hence a decline in lithium-ion diffusion capability, likely due to the

higher mass loading and greater tortuosity in the denser electrode.

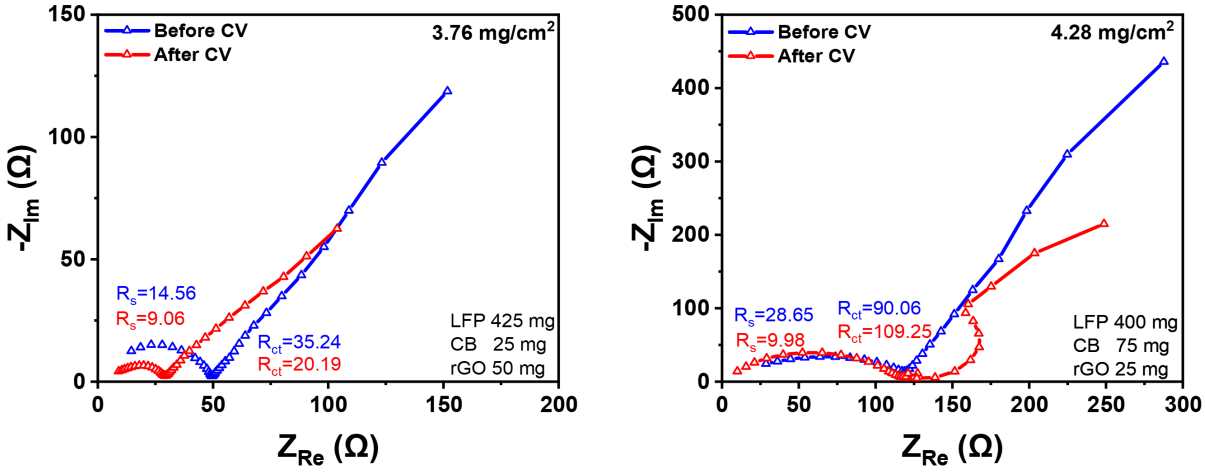

Figure 4.8: a) KK71 EIS plot. b) KK93 EIS plot.

When comparing the two samples, it becomes evident that the KK71 electrode, with a moderate areal loading of 3.76mg/cm^2 (LFP 425mg, CB 25mg, rGO 50mg), exhibited overall superior electrochemical characteristics after CV activation. Specifically, it displayed lower R_s and R_{ct} values, as well as a steeper low-frequency tail, all indicative of enhanced ionic conductivity, improved charge transfer kinetics, and more efficient lithium-ion diffusion. In contrast, the KK93 electrode, despite its slightly higher loading of 4.28mg/cm^2 (LFP 400mg, CB 75mg, rGO 25mg), showed increased R_{ct} and a more depressed diffusion tail after CV, suggesting compromised charge transfer and slower ion transport.

The overall internal resistance of KK71 is lower than that of KK93, which may be attributed to the reduction of CB and the increased content of rGO. Excessive carbon black can lead to poor dispersion during initial deposition, thereby compromising coating uniformity. In contrast, an appropriate increase in rGO content improves suspension stability and coating homogeneity. Furthermore, the porous architecture of rGO offers additional lithium-ion transport pathways, effectively reducing the overall structural resistance and enhancing electrochemical performance. Therefore, a moderate increase in rGO content can contribute to reducing the overall internal resistance of the battery. However, the optimal rGO loading for achieving the best electrochemical performance of the cathode electrode requires further investigation.

4.3.3 Galvanostatic Charge–Discharge

Galvanostatic charge–discharge (GCD) testing is a standard electrochemical technique used to evaluate the practical capacity, rate capability, and electrochemical stability of electrode materials. By applying a constant current density (expressed as a C-rate), the charge and discharge potential profiles provide key insights into ion intercalation behavior, internal resistance, and polarization losses of lithium-ion battery electrodes. The shape and retention of voltage plateaus across different C-rates directly reflect the electrochemical kinetics and the accessibility of active materials during cycling.

GCD testing was conducted at multiple C-rates—0.05C, 0.1C, 0.2C, 0.5C, and 1C—with the first 10 cycles performed at 0.05C to stabilize electrochemical interfaces, followed by 5 cycles at each subsequent rate. Notably, the KK93 electrode was only tested up to 0.5C, whereas KK58 was tested through to 1C.

As shown in Figure 4.9, both KK58 (a) and KK93 (b) electrodes display flat voltage plateaus characteristic of $LiFePO_4$ redox reactions. In the low-to-moderate C-rate range (0.05C to 0.2C), the KK93 electrode delivers consistently higher specific capacities than KK58. For example, at 0.05C, KK93 approaches nearly 95 mAh/g, compared to approximately 85 mAh/g for KK58. Similarly, at 0.1C and 0.2C, KK93 continues to show broader charge/discharge profiles and extended plateaus, suggesting more efficient lithium-ion intercalation under slow current conditions. However, when the current rate increases beyond 0.2C, both electrodes exhibit signs of instability. In KK93, the voltage plateau at 0.5C rapidly drops toward the cut-off voltage, indicating increased polarisation and internal resistance, despite its initially higher capacity. KK58, although able to operate at 1C, also shows increased polarisation and reduced discharge capacity, reflecting limitations in reaction kinetics under fast charge/discharge conditions. This high-rate instability in both electrodes may be attributed to several factors: insufficient ion diffusion at higher current densities, limited electronic conductivity across thicker or more compact electrode structures, and incomplete utilisation of active material due to restricted lithium-ion transport.

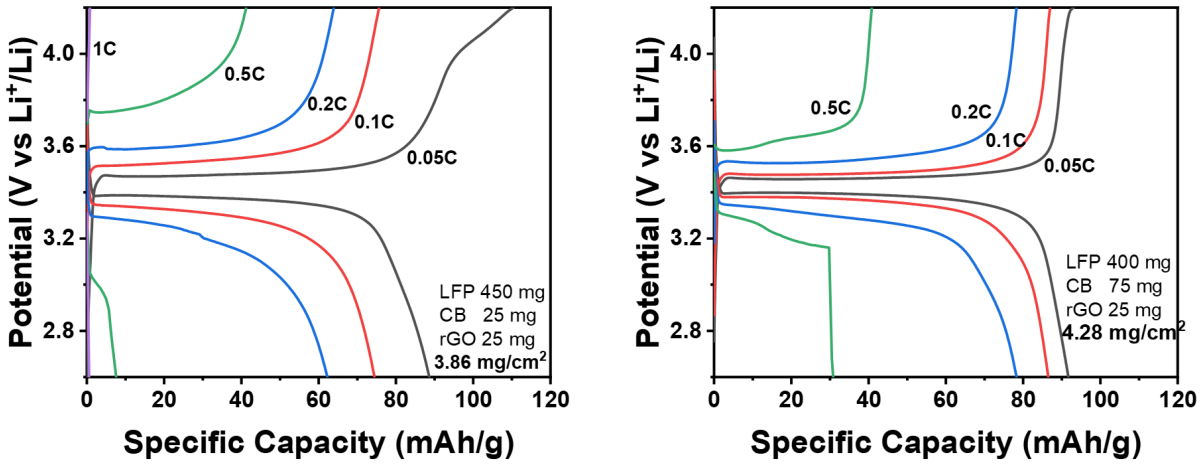

Figure 4.9: a) KK58 GCD plot. b) KK93 GCD plot.

The observed differences in discharge capacity and rate performance can be attributed primarily to variations in CB content. The KK93 electrode contains a higher amount of CB (75 mg) compared to KK58 (25 mg), while the rGO content remains constant at 25 mg in both samples. The increased CB loading in KK93 enhances the electronic conductivity of the electrode, effectively reducing internal resistance and facilitating electron transport during charge–discharge processes. This improved conductivity is reflected in the higher specific capacities observed for KK93 across all tested C-rates (0.05C to 0.5C), indicating more efficient utilisation of the active material under both low and moderate current conditions. Since the rGO content is identical in both electrodes, its influence on performance can be considered negligible in this comparison. Therefore, the improved rate performance of KK93 is primarily attributed to the enhanced electronic conductivity

provided by the elevated CB content.

5

Conclusion

"The important thing is not to stop questioning. Curiosity has its own reason for existence."

— Albert Einstein

This thesis explored the application of electrophoretic deposition (EPD) as a scalable and versatile fabrication technique for developing multifunctional cathode electrodes in structural batteries. The research was motivated by the increasing demand for integrated systems that combine energy storage and structural functionality, particularly in aerospace, automotive, and portable electronics applications. Carbon fibre (CF) was employed as the structural substrate due to its low density, high mechanical strength, and inherent conductivity, making it an ideal candidate for multifunctional integration.

The study addressed four key objectives: (1) investigating the effect of magnetic field assistance during the EPD process; (2) enhancing fabrication efficiency through the design and testing of high-throughput sample holders; (3) extending EPD to electromagnetic interference (EMI) shielding applications via Fe_3O_4-based composites; and (4) evaluating the electrochemical performance of LFP-based CF cathodes with varying rGO content.

In the first part of the study, magnetic field-assisted EPD was shown to improve deposition quality under specific compositional conditions. SEM imaging confirmed more uniform and denser coatings when a magnetic field was applied, particularly in low-agglomeration suspensions. However, excessive CB or rGO content led to particle clustering, limiting the beneficial effects of the magnetic field. This highlights the importance of balancing material ratios and maintaining suspension stability during the deposition process.

The second major contribution involved improving fabrication throughput. By developing and comparing two-, three-, and four-electrode holder systems, the study found that the three-electrode configuration offered an optimal balance between efficiency and deposition quality. The redesign reduced the time needed to prepare 10 samples from over 3 hours to under 1 hour, significantly increasing productivity while maintaining coating uniformity.

The third experimental focus expanded the applicability of EPD to EMI shielding by incorporating Fe_3O_4 into the suspension. Although full EMI performance testing could not be completed within the scope of this work, the successful deposition of Fe_3O_4 on CF demonstrates the feasibility of fabricating dual-functional electrodes. Literature reports support Fe_3O_4's effectiveness in EMI shielding when combined with conductive or porous substrates, and this study contributes to that research by introducing CF as a potential

high-performance carrier.

Lastly, the electrochemical evaluation of LFP/CB/rGO electrodes revealed that moderate rGO content (50 mg) improved charge transfer and reduced internal resistance, as shown by EIS and CV testing. However, high rGO levels (75 mg) resulted in poor dispersion and uneven coatings, negatively affecting electrode performance. These results underscore the need for compositional optimization to balance conductivity, uniformity, and long-term stability.

In conclusion, this work demonstrates that EPD is a viable method for producing high-performance structural battery cathodes, with potential for multifunctional integration including EMI shielding. The magnetic field-assisted EPD and high-throughput modifications provide valuable insights into scalable fabrication strategies. While some performance aspects, such as EMI shielding efficiency, require further investigation, the study offers a solid foundation for future research into lightweight, multifunctional energy systems.

Bibliography

[1] P. Rüetschi, "Review on the lead-acid battery science and technology," *Journal of Power Sources*, vol. 2, no. 1, pp. 3-120, Dec. 1977, doi: 10.1016/0378-7753(77)85003-9.

[2] M. S. Whittingham, "Materials Challenges Facing Electrical Energy Storage," *Proceedings of the IEEE*, vol. 100, no. 5, pp. 1518-1534, 2012, doi: 10.1109/JPROC.2012.2190170.

[3] A. Manthiram, "A Reflection on Lithium-Ion Battery Cathode Chemistry," *ACS Central Science*, vol. 3, no. 10, pp. 1063-1069, 2017, doi: 10.1021/acscentsci.7b00288.

[4] L. Asp, K. Bouton, D. Carlstedt, S. Duan, R. Harnden, W. Johannisson, M. Johansen, M. Johansson, G. Lindbergh, F. Liu, K. Peuvot, L. M. Schneider, J. Xu, and D. Zenkert, "A Structural Battery and its Multifunctional Performance," *Advanced Energy and Sustainability Research*, vol. 2, no. 3, p. 2000093, 2021. doi: 10.1002/aesr.202000093.

[5] R. Pejman, J. Gorman, and A. R. Najafi, "Multi-physics design of a new battery packaging for electric vehicles utilising multifunctional composites," *Composites Part B: Engineering*, vol. 237, p. 109810, 2022. doi: 10.1016/j.compositesb.2022.109810.

[6] H. Kuehnelt, A. Beutl, F. Mastropierro, F. Laurin, S. Willrodt, A. Bismarck, M. Guida, and F. Romano, "Structural Batteries for Aeronautic Applications—State of the Art, Research Gaps and Technology Development Needs," *Aerospace*, vol. 9, no. 1, p. 7, 2022. doi: 10.3390/aerospace9010007.

[7] European Union, "Regulation (EU) 2021/1119 of the European Parliament and of the Council of 30 June 2021 establishing the framework for achieving climate neutrality and amending Regulation (EC) No 401/2009 and (EU) 2018/1999," *Official Journal of the European Union*, vol. L 243, pp. 1–17, 2021. doi: 10.3000/9789276348317.

[8] J. A. Arfwedson, "Untersuchung einiger bei der eisen-grube von utö vorkommenden fossilien und von einem darin gefundenen neuen feuerfesten alkali," *Journal of Chemical Physics*, vol. 22, pp. 93–117, 1818.

[9] J. J. Berzelius, "Ein neues mineralisches alkali und ein neues metall," *Journal of Chemical Physics*, vol. 21, pp. 44–48, 1817.

[10] W. T. Brande, *A Manual of Chemistry*, 2nd ed., vol. 2, pp. 57–58, John Murray,

London, UK, 1821.

[11] T. Nagaura, M. Nagamine, I. Tanabe, and N. Miyamoto, "Solid-state batteries with sulfide-based electrolytes," *Progress in Batteries and Solar Cells*, vol. 8, pp. 84–88, 1989.

[12] T. Nagaura and K. Tozawa, "Lithium-ion rechargeable battery," *Progress in Batteries and Solar Cells*, vol. 9, pp. 209–212, 1990.

[13] Y. Nishi, "Lithium ion secondary batteries: Current status and future prospects," *Journal of Power Sources*, vol. 100, no. 1-2, pp. 101-106, 2001.

[14] L. Zhang, et al., "Recent advances in high-performance cathode materials for lithium-ion batteries," *Materials Science and Engineering: R: Reports*, vol. 138, pp. 14-29, 2019.

[15] M. Armand and J. M. Tarascon, "Building better batteries," *Nature*, vol. 451, no. 7179, pp. 652-657, 2008.

[16] J. B. Goodenough and K. S. Park, "The Li-ion rechargeable battery: A perspective," *Journal of the American Chemical Society*, vol. 135, no. 4, pp. 1167-1176, 2013.

[17] L. E. Asp and E. S. Greenhalgh, "Structural power composites," *Composites Science and Technology*, vol. 101, pp. 41-61, 2014, doi: 10.1016/j.compscitech.2014.06.020.

[18] E. Jacques, "Lithium-intercalated carbon fibres towards the realisation of multifunctional composite energy storage materials," PhD thesis, KTH School of Engineering Sciences, 2014.

[19] A. Marchenko and H. Kavatsiuk, "Advancing Structural Batteries using Lithium-Iron Phosphate Functionalised High-Modulus Carbon Fibres Positive Electrodes," Master's thesis, Chalmers University of Technology, Gothenburg, Sweden, 2024.

[20] J. Choi, O. Zabihi, M. Ahmadi, and M. Naebe, "Advancing structural batteries: cost-efficient high-performance carbon fibre-coated $LiFePO_4$ cathodes," *Journal of Materials Chemistry A*, vol. 11, pp. 15064–15075, 2023. doi: 10.1039/D3TA01359C.

[21] A. del Bosque, D. Vergara, G. Lampropoulos, and P. Fernández-Arias, "Energy Storage in Carbon Fiber-Based Batteries: Trends and Future Perspectives," *Batteries*, vol. 10, no. 3, pp. 85, 2024. doi: 10.3390/batteries10030085.

[22] J. S. Sanchez et al., "Electrophoretic coating of $LiFePO_4$/graphene oxide on carbon fibres as cathode electrodes for structural lithium ion batteries," *Composites Science and Technology*, vol. 208, 108768, 2021. doi: 10.1016/j.compscitech.2021.108768.

[23] A. Hajizadeh et al., "Electrophoretic deposition as a fabrication method for Li-ion battery electrodes and separators – a review," *Journal of Power Sources*, vol. 535, 231448, 2022. doi: 10.1016/j.jpowsour.2022.231448.

[24] H. Zhang, X. Liu, J. Zhang, X. Li, Y. Wang, and J. Shi, "Preparation and characterization of novel porous ceramic membranes for oil-water separation," *Ceramics In-*

ternational, vol. 40, no. 5, pp. 7057–7065, 2014. doi: 10.1016/j.ceramint.2014.01.043.

[25] D. D. L. Chung, "Materials for electromagnetic interference shielding," *Materials Chemistry and Physics*, vol. 255, p. 123587, 2020. doi: 10.1016/j.matchemphys.2020.123587.

[26] E. Mikinka and M. Siwak, "Recent advances in electromagnetic interference shielding properties of carbon-fibre-reinforced polymer composites—a topical review," *Journal of Materials Science: Materials in Electronics*, vol. 32, pp. 24585–24643, 2021. doi: 10.1007/s10854-021-06900-8.

[27] S. Saini et al., "Shielding the Future: The Role of Innovative Materials in Electromagnetic Interference Mitigation," *Journal of Alloys and Compounds*, vol. 1022, p. 179969, 2025. doi: 10.1016/j.jallcom.2025.179969.

[28] E. I. Nduka et al., "Effect of magnetic field on the rate performance of a Fe_2O_3/$LiFePO_4$ composite cathode for Li-ion batteries," *RSC Advances*, vol. 14, pp. 36005–36015, 2024. doi: 10.1039/D4RA06707J.

[29] Z. Ma, D. Kong, Y. Fan, and H. Xu, “A review of electrophoretic deposition of carbon nanotubes and carbon nanotube-based composites,” *Carbon Resources Conversion*, vol. 1, no. 1, pp. 2–15, 2018. doi:10.1016/j.crcon.2018.05.001.

[30] X. Caldentey and E. Romero, "High-Throughput Experimentation as an Accessible Technology for Academic Organic Chemists in Europe and Beyond," *Chemistry–Methods*, vol. 3, no. 6, p. e202300020, 2023. doi: 10.1002/cmtd.202300020.

[31] L. M. Mayr and D. Bojanic, "Novel trends in high-throughput screening," *Current Opinion in Pharmacology*, vol. 9, no. 5, pp. 580–588, 2009. doi: 10.1016/j.coph.2009.08.004.

[32] R. Chaudhary, J. Xu, Z. Xia, and L. E. Asp, "Unveiling the Multifunctional Carbon Fibre Structural Battery," *Advanced Functional Materials*, vol. 32, no. 38, pp. 2204172, 2022. doi: 10.1002/adfm.202204172.

[33] M. Bayat, H. Yang, F. Ko, and D. G. Michelson, "Electromagnetic Interference Shielding Effectiveness of Hybrid Multifunctional Fe_3O_4/Carbon Nanofiber Composite," *Polymer*, vol. 55, no. 3, pp. 936–943, 2013. doi: 10.1016/j.polymer.2013.12.040.

[34] K. Yu et al., "rGO/Fe_3O_4 hybrid induced ultra-efficient EMI shielding performance of phenolic-based carbon foam," *RSC Advances*, vol. 9, no. 36, pp. 20643–20651, 2019. doi: 10.1039/C9RA03659B.

[35] A. C. Sparavigna, "Iron Oxide Fe_3O_4 Nanoparticles for Electromagnetic Shielding," *ChemRxiv*, preprint, 2023. doi: 10.26434/chemrxiv-2023-4w31q.

[36] J. S. Sanchez, A. Mendoza, F. González, A. Lozano, and M. Anglada, "Electrophoretic coating of $LiFePO_4$/graphene oxide on carbon fibres as cathode electrodes for structural lithium-ion batteries," *Composites Science and Technology*, vol. 208, p. 108768, 2021. doi: 10.1016/j.compscitech.2021.108768.

DEPARTMENT OF SOME SUBJECT OR TECHNOLOGY
CHALMERS UNIVERSITY OF TECHNOLOGY
Gothenburg, Sweden
www.chalmers.se

CHALMERS
UNIVERSITY OF TECHNOLOGY